Computational Fluid Dynamics Modeling of Cough Transport in an Aircraft Cabin

Angela C. Davis[a], Malia Zee[a], Andrew D. Clark[a], Tateh Wu[a], Stephen P. Jones[a], Lindsay L. Waite[a], Joshua J. Cummins[a], Nels A. Olson[a,*].

[a]The Boeing Company, 100 N Riverside, Chicago, IL 60606.
[*]Correspondence to: Nels A. Olson, nels.a.olson@boeing.com.

Abstract

To characterize the transport of respiratory pathogens during commercial air travel, Computational Fluid Dynamics simulations were performed to track particles released by coughing from a passenger seated in different seats on a Boeing 737 aircraft. Simulation data were post-processed to calculate the amounts of particles inhaled by nearby passengers. Different airflow rates were used, as well as different initial conditions to account for random fluctuations of the flow field. Overall, 80% of the particles were removed from the cabin in 1.3 to 2.6 minutes, depending on conditions, and 95% of the particles were removed in 2.3 to 4.5 minutes. Reducing airflow increased particle dispersion throughout the cabin but did not increase the highest exposure of susceptible passengers. The highest exposure was 0.3% of the total nonvolatile mass emitted by the cough, with average exposure of 0.05%, in line with recent experimental testing reported in literature.

Introduction

The COVID-19 pandemic has created a global health and economic crisis. While vaccines reported to have high short-term efficiencies against the current variants of SARS-CoV-2 have been approved by U.S., E.U., and other regulatory authorities, and initial doses are being distributed to the general population, large-scale vaccination is expected to be slow, and uncertainty remains about vaccine effectiveness in the long term and against newly emerging variants of the coronavirus. In this context, it is imperative to assess the risks of disease transmission due to various common activities to enable individuals to make informed decisions about engagement. Air travel is one such activity.

Although highly symptomatic COVID-19 carriers are unlikely to be on commercial aircraft due to current airline travel policies, asymptomatic and presymptomatic carriers continue to travel, and mildly symptomatic carriers who are able to board undetected do so with some regularity.

According to contact tracing organizations [1], this often occurs when the subject becomes infected while away on travel, and travels while potentially symptomatic in order to return home. Nonetheless, reports of COVID-19 transmission onboard aircraft are rare, with no confirmed cases for domestic travel within the U.S. at the time of this writing, despite 1,600 cases of potentially symptomatic travelers that have been investigated by the Center for Disease Control and Prevention [1]. Since contact tracing is difficult when travel is involved due to the decentralized structure of the current efforts, the present study was performed in order to complement the epidemiological data.

The expiratory activity selected for study was a single cough, because it is a higher-magnitude perturbation than either breathing or talking in terms of both the number and the volume of expiratory particles, as well as in terms of momentum, which is expected to translate to a greater challenge to particle removal by the aircraft. Sneezing, which is a higher-magnitude perturbation than coughing, was not selected for study because it is not a symptom of COVID-19 [2]. Computational Fluid Dynamics (CFD) analysis was performed to predict material transport during and after the cough discharge, and material inhaled by other passengers was used to quantify passenger exposure – or, viewed alternately, to characterize the efficiency of the aircraft system at protecting passengers from exposure to infectious material.

Airflow Design

While the air handling system on modern aircraft provides far better protection against airborne pathogens than the vast majority of other common environments, its design has been motivated by passenger comfort and the large cooling requirements of the on-board electronics systems.

Under most conditions, air supplied to the aircraft cabin is a mixture of outside air with air removed from the cabin, which is filtered before it is recirculated. Recirculation is used both to improve fuel efficiency and to increase humidity, which plays a role in passenger comfort. As a rare exception, during ground operations, no outside air may be available, in which case, all air supplied to the cabin is the filtered recirculated air. Either scenario provides high-purity air through the use of high-efficiency particulate air (HEPA) filters, which remove 99.97% of particles at 0.3 μm, a filtration level that is sufficient to remove viruses that are contained in droplet nuclei of respiratory emissions. The outside air is assumed to be free of pathogens, and its pressure, temperature, and humidity are adjusted to comfortable levels on the way to the cabin by either the Environmental Control System (ECS) or the ground supply sources.

Air is introduced into the passenger cabin through air distribution nozzles which are typically located above the seats to maximize thermal comfort for passengers and the crew. On the 737 interior used in the current study, air distribution nozzles are located outboard of the Passenger Service Unit (PSU) and direct the airflow inboard toward the center of the cabin, Fig. 1. The supply airstream remains attached to the PSU and the stow bin through the Coandă effect [3].

On reaching the aisle, the airstream combines with the opposing airstream and in the process redirects toward the floor, producing higher velocities in the aisle compared to the seated sections, which compartmentalizes the left and right sections into cells. At the floor, the stream splits and continues outboard to either side of the cabin and toward the return air grilles, with low pressure behind the grilles driving the motion. Air which does not exit through the grilles rises by buoyancy due to heat sources from the passengers and the In-Flight Entertainment Systems and becomes entrained in the high-velocity jet at the air distribution nozzle. Then the process repeats again.

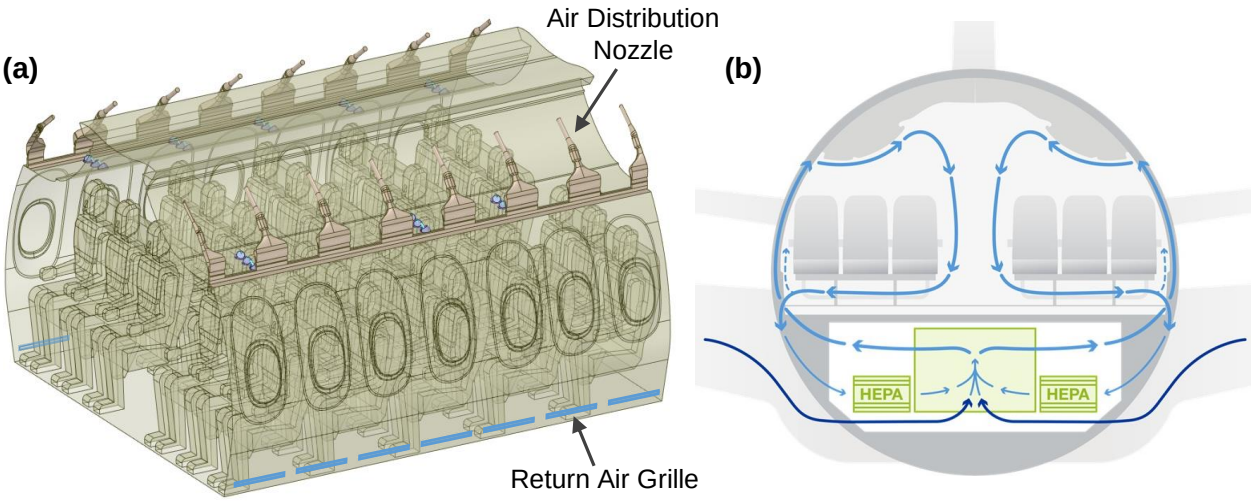

Fig. 1. Airflow design in narrow-body aircraft. **(a)** Airflow delivery features in the 737 Boeing Sky Interior cabin used in simulations. **(b)** Idealized airflow pattern in the passenger cabin.

The resulting airflow pattern consists of two counter-rotating cells formed around the rows of passenger seating. High seat backs support the cohesion of the cell structure and limit fore-aft movement. This compartmentalized design was originally developed during the era when inflight smoking had been the norm, as a means to reduce exposure to second-hand smoke of the passengers and the flight crew. Since cigarette smoke has particles in a similar size range as expiratory emissions, this design was also expected to limit the spread of potentially infectious particles in the era of COVID-19.

Simulation Overview

Simulations were performed in a 5-row, 30-seat section of the 737 Boeing Sky Interior cabin with periodic front and back interfaces, Fig. 1(a). Forward-facing passengers occupied all seats. Personal Air Outlets were left off due to large variability in available PAO positioning and the absence of a recommendation for PAO use in the COVID-19 context. A breathing zone was defined around the face of each passenger to track particle exposure, as shown in Supplementary Fig. S1. The size of the breathing zone was 1 ft on each side, or 0.8 ft^3 due to volume occupied by each passenger's face.

Supplementary Table S1 summarizes the simulated cases, which varied the seat position of the coughing index passenger, the airflow rate, and the randomly generated initial condition. One airflow rate was studied with initial conditions from three different time points to reflect the right-to-left shifts in the counter-rotating cell structure that occur on a periodic basis, as shown in Fig. 2. Separate initial steady-state solutions were required for each airflow rate and are indicated in the case table.

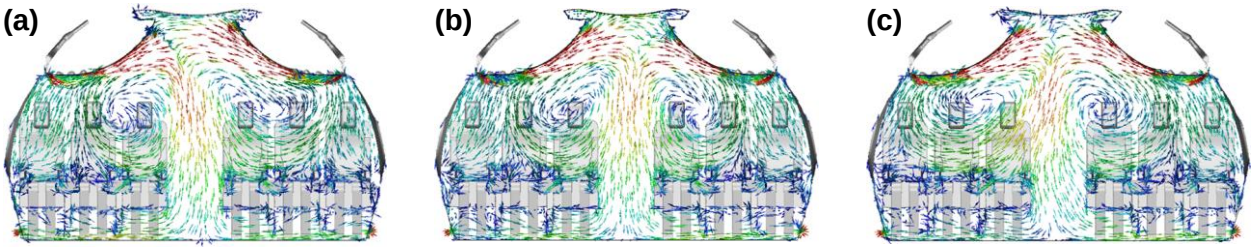

Fig. 2. Velocity vectors of initial conditions at 100% flow rate with the highest velocities shown in red and the lowest ones in blue. Time offset and initial condition index as follows: **(a)** 0 s, Initial Condition 1, **(b)** 90 s, Initial Condition 2, **(c)** 120 s, Initial Condition 3.

Results

Particle Removal Dynamics

Overall cough particle dynamics were tracked by following the decay in the number of expiratory particles over the course of each simulation, Fig. 3. The initial features on the decay curves corresponded to deposition onto surfaces such as the seat back in front of the index subject. Approximately 50% of the nonvolatile content was deposited on various surfaces, with the rest removed through the return air grilles located near the floor on the interior walls.

Differences due to random fluctuations of the flow field were captured effectively by differences in starting conditions. These random differences affected the rate of particle removal from the

cabin over the first 1-2 minutes, Fig. 3(a), but their effect decreased with time, and the final time for particle removal was independent of the initial condition. For example, for an index passenger in seat 3D with airflow at 100%, initial conditions resulted in a 3-second (0.05 minute) difference in the time to reach 95% removal of particles from the cabin, which was 2.4 minutes.

Supply airflow rate, on the other hand, had a large effect on the rate of particle removal, Fig. 3(b). At 100% flow rate, 95% of the particles were removed in 2.3 to 2.5 minutes (80% in 1.3 to 1.4 min, 99% in 3.3 to 3.5 min). At 55% flow rate, it took 4.5 minutes to reach 95% removal of particles (80% in 2.6 min, 99% in 6.3 minutes).

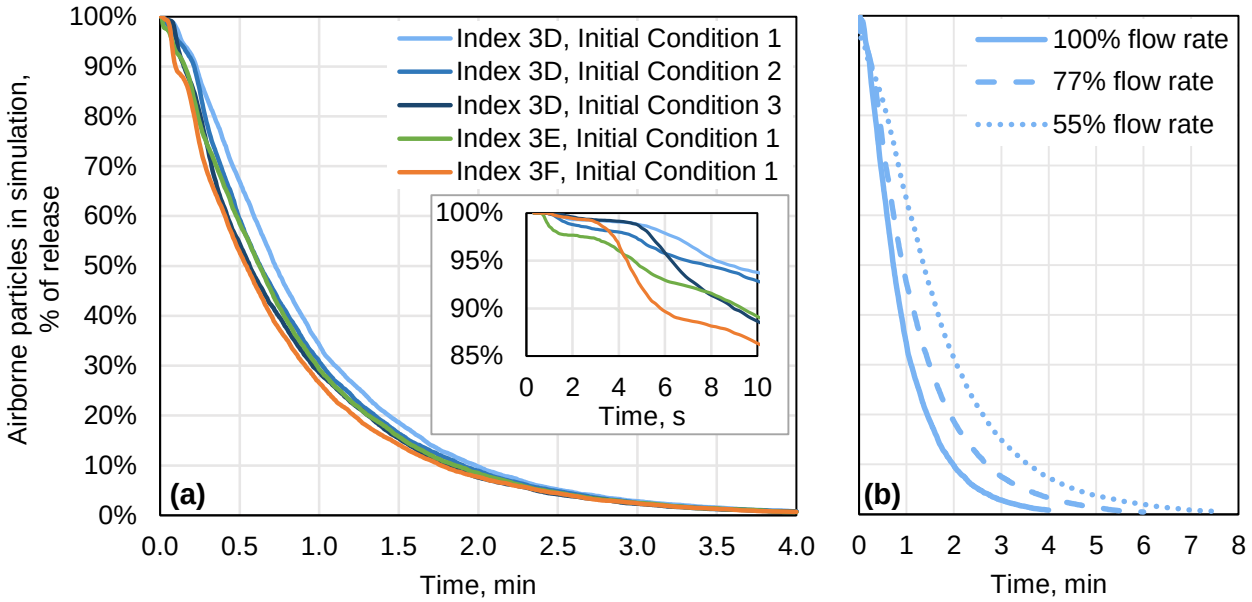

Fig. 3. Decay of expiratory particles over time after initial release. **(a)** Airflow at 100% with different index seats and initial conditions. **(b)** Airflow at 55-100% with index subject in aisle seat 3D.

Particle dynamics in the breathing zones of susceptible passengers were tracked by following particle masses over time, Fig. 4. All particles were dehydrated by the time they reached the nearby breathing zones, so their masses are expressed as a percentage of the original nonvolatile content. Particle decay in a given breathing zone was faster than the overall rate of particle removal. For example, for an index passenger in seat 3E, susceptible passenger in seat 3D, and 100% airflow, 95% of the cumulative nonvolatile mass was removed in 1.4 minutes (80% in 0.7 min, 99% in 2.3 min). A seat chart is provided in Fig. 5.

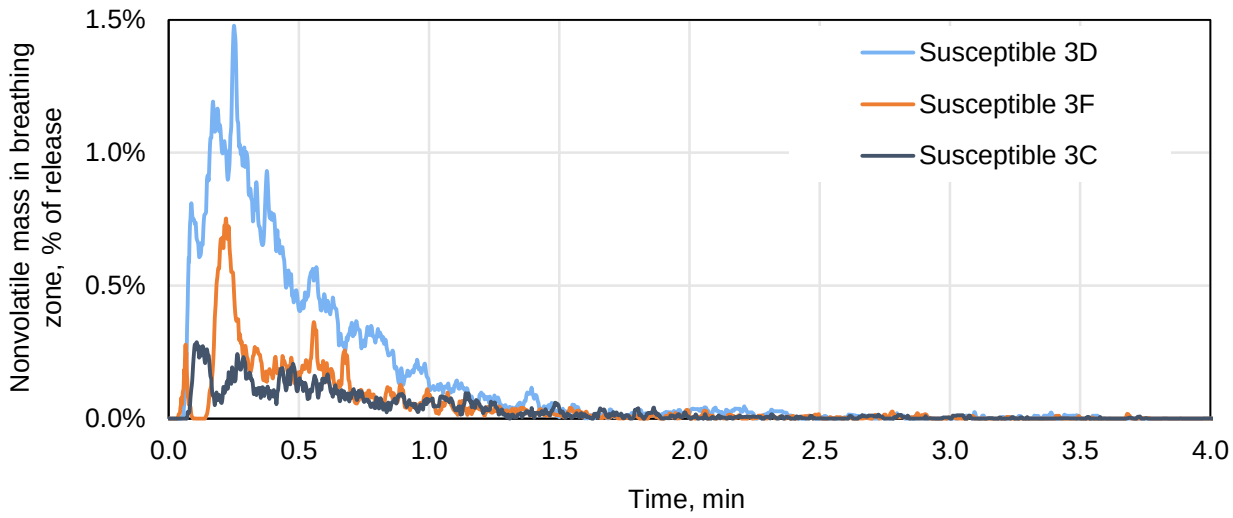

Fig. 4. Mass of expiratory material released by index passenger in middle seat 3E and present in the breathing zones of susceptible subjects in nearby seats over time after initial release.

1A	1B	1C
2A	2B	2C
3A	3B	3C
4A	4B	4C
5A	5B	5C

1D	1E	1F
2D	2E	2F
3D	3E	3F
4D	4E	4F
5D	5E	5F

Fig. 5. Seat chart for the 5-row section used in the model, highlighting seats occupied by the index subject in different simulations.

Inhaled Mass

Inhaled mass in each susceptible passenger's breathing zone was integrated over the course of each simulation, with cumulative exposures presented in Fig. 6. In general, passengers seated closer to the index seat had a higher exposure to index expiratory material than those farther away. Exposure was highest for passengers seated in the index subject's row, and lowest for passengers seated two rows away. Exposure was higher on the right side of the cabin, where the index passenger's seat was located, than on the opposite side. This is consistent with the counter-rotating cell pattern of airflow depicted schematically in Fig. 1(b) and Fig**. 2**.

Exposure of susceptible passengers in the index subject's row was lowest when the index subject was in the window seat. Exposure of passengers in the window seat was lower than exposure of passengers in the aisle seat. However, all exposures were a small fraction of the amount released: the maximum mass inhaled by a susceptible passenger was 0.3% (Supplementary Figs. S2 and S3). This occurred for index passenger in seat 3E and susceptible passenger in seat 3D, with dynamics shown in Fig. 4. Differences due to random fluctuations of the flow field when the index subject was in the aisle seat had a substantial effect on exposure for some of the seats, with the maximum coefficient of variance of 45%, which occurred for susceptible passenger in seat 3F. The minimum coefficient of variance was 5.4% and the average was 19%.

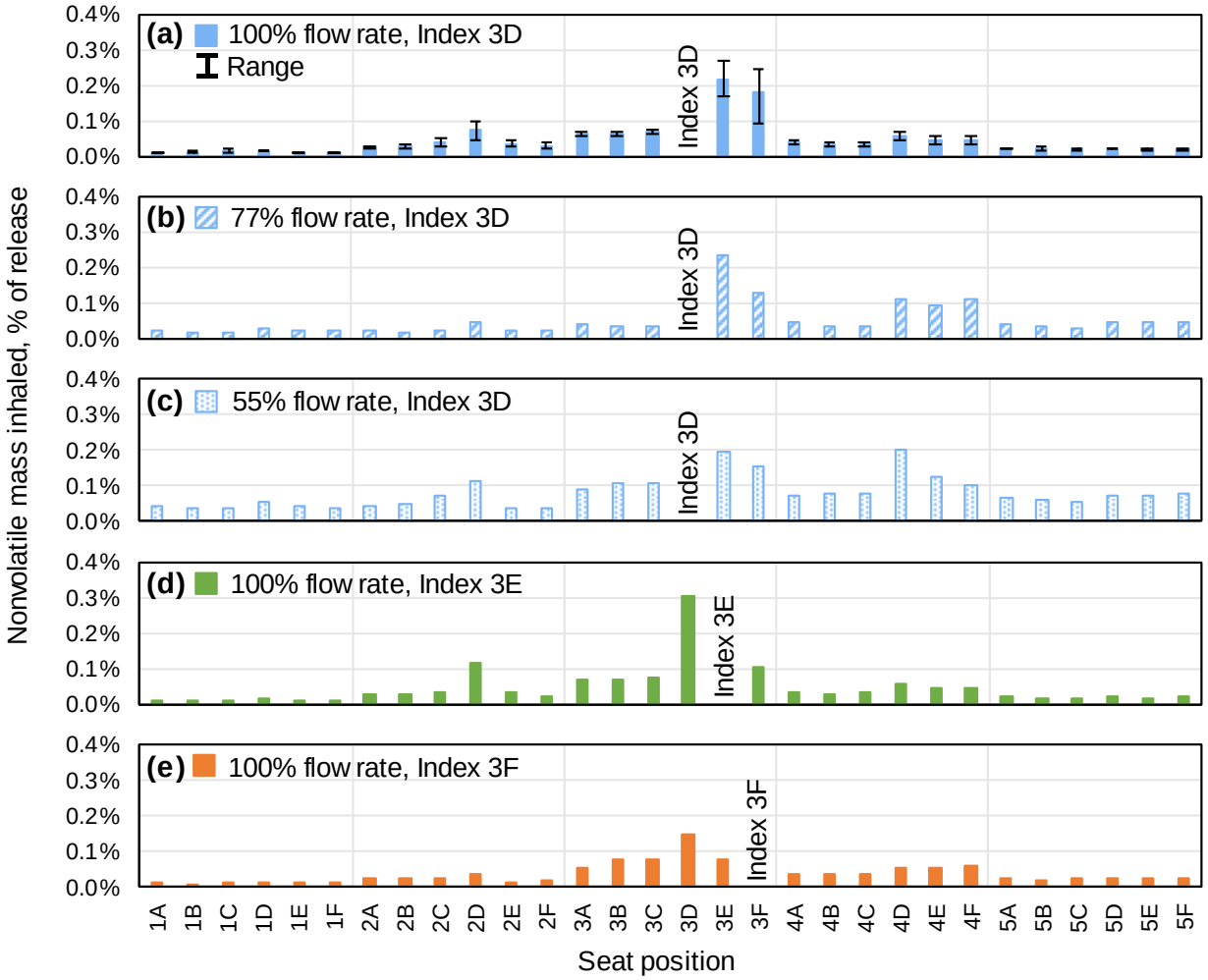

Fig. 6. Mass of expiratory material inhaled by susceptible subjects in different seats for different airflow conditions **(a-c)** and different index passenger seat positions at 100% airflow **(a, d-e)**. Error bars in **(a)** represent the range over three different initial conditions.

Reducing airflow from 100% to 55% resulted in a wider spread of particles throughout the cabin, observed as an increase of inhaled mass for all rows in Fig. 6(c) compared to Fig. 6(a). For most passengers, exposure increased as airflow was reduced. As one exception, when airflow was reduced to 77%, exposure of seats 3A-C slightly decreased. However, this exception is thought to be due to random differences in initial conditions used for each airflow rate.

Discussion

Transport of particles expelled by a single cough was studied to characterize the effectiveness of airplane ventilation and airflow patterns in protecting passengers from exposure to an infected index subject. This case was studied both as a perturbation to quantify the efficiency of the aircraft system in removing particles from the passenger cabin, and as a scenario that currently commands public interest.

The amount of respiratory material inhaled by susceptible passengers was quantified in terms of nonvolatile mass and expressed as a percentage of the nonvolatile mass expelled by the index subject. This material transport approach is not specific to any disease, and was used because the input data required for a disease transmission model of SARS-CoV-2 is not currently available. Specifically, the distribution of SARS-CoV-2 across particles of different sizes is not known, but is likely non-uniform: for example, influenza is shed predominantly in smaller particles [4,5,6] even though larger particles account for the bulk of the expelled volume. Smaller particles also may be more infectious, as they may deposit deeper in the respiratory tract upon inhalation. For influenza, the infectious dose may be as much as two orders of magnitude lower for inoculation by inhaled aerosol vs. intranasal drops [7]. These factors are important here because particles of different sizes have different aerodynamic behaviors, so the absence of inputs specific to SARS-CoV-2 creates a limitation.

Viewed alternatively, the current material transport approach is equivalent to making the simplifying assumptions that the pathogen of interest is uniformly distributed across particles of different sizes, and that the infectious dose is independent of particle size. Given those assumptions, the exposure of susceptible subjects in terms of a percentage of nonvolatile mass expelled would be equivalent to the percentage of viruses expelled, which could then be related to virus shedding rates and infectious doses to extend the present work to a disease transmission model. However, this disease transmission model was not examined in the present work because of a low certainty that these simplifying assumptions are valid.

Nonetheless, a key finding of the present research was that the exposure to respiratory particles expelled by the index passenger was low even for the nearest neighbors, with a maximum exposure of 0.3% of the nonvolatile mass expelled. The amount inhaled by the susceptible passengers depended primarily on their proximity to the index subject and on airflow rate, with random fluctuations of the flow field also having a significant role. Humidity did not have a substantial effect within the low-humidity range that is typical of cruise altitudes, Supplementary Figs. S4 through S6.

Three airflow cases were studied that cover the range of airflow rates that would be expected over the course of a journey, with 77% being the average. The lowest flow rate studied, 55%, may occur on the ground during the boarding and deplaning segments, when both the engines and the auxiliary power unit (APU) are off, and no ground air supply is available. While this scenario is less common, it provided a lower bound airflow rate for calculating exposures of susceptible passengers to an infected index person. Decreasing the airflow rate increased the dispersion of expiratory particles in the cabin, but did not increase the maximum exposure to the expiratory material. While exposures of passengers seated away from the index subject increased, exposures of the index's neighbors remained the same within the variability caused by random flow field fluctuations. For passengers seated away from the index subject, exposure remained on par or lower than exposure of passengers seated in the same triplet of seats as the index.

Experimental Comparison

The present results are broadly consistent with the results of experimental work [8] that was funded by the United States Transport Command (TRANSCOM) Air Mobility Command (AMC) division of the US Military, and was planned and carried out by a large team that included some of the authors of the present paper. In that work, tracer aerosols were released at various seat locations throughout Boeing 777-200 and 767-300 airframes, both on the ground and in flight, and were measured at 40+ sensor locations for each release of ~180 million particles over a 1 minute period. A total of over 300 releases were performed. Exposure levels of susceptible passengers were below 0.1% in the vast majority of cases, which was lower than exposure levels in the present model.

The results of this study and those by the TRANSCOM/AMC team were within the same order of magnitude, and the differences are thought to be due to some of the methodological differences, which are summarized in Table 1. Twenty-five percent of the difference is explained by the choice of a larger minute volume in the model (which is the volume of air that is inhaled or

exhaled in one minute). The value in the TRANSCOM/AMC work was selected to represent an average property across the population, while the value here was selected to represent an individual on the higher end of the distribution. In general, minute volume, and therefore, the amount of material inhaled depends on gender, age, body mass, and individual factors; however, whether minute volume affects disease transmission is not yet well understood. The present model used a value on the higher end of the distribution as a conservative assumption. For the same reason, no provision was made to re-exhale a fraction of the inhaled material.

While the choice of minute volume explains a fraction of the difference, other factors must account for the remainder. One possibility is that, since the experimental releases represented breathing rather than coughing and were thus performed at a slower rate, they presented less of a challenge to the ventilation and air handling system than a cough due to their lower inertia, and were removed from the cabin with greater efficiency. Another possibility is that the differences in particle properties or in thermal output of susceptible subjects played a role. A validation study would be required to assess these factors.

Finally, differences due to random fluctuations of the flow field had a larger effect on model results than on TRANSCOM/AMC testing. This can be explained by differences in release durations. Since the particles were released over a longer time period in the experimental work, over 1 minute compared to 0.4 seconds, and the random fluctuations cases studied in the model were on the order of 30 to 120 seconds, much of the effect of random fluctuation was averaged out in experimental testing.

Table 1. Comparison of methods and results in the present work to experimental aerosol releases performed by the TRANSCOM/AMC team [8].

	Property	**Present Model**	**Experimental**
Aircraft	Airframe	Boeing 737-800 NG or Boeing 737-8 MAX	Boeing 777-200 and Boeing 767-300
	Airframe type	Narrow-body	Wide-body
	Airflow rate	55%, 77%, 100%	Similar to 77%
	Personal Air Outlets	Off	Off in 85% of cases
Expiratory Particles	Size distribution	Poly-dispersed, based on voluntary coughs of healthy volunteers	Narrowly-disperse, nominal 1μm
	Nonvolatile fraction	10%	Polystyrene latex beads in water
	Interactions with surfaces	100% adhesion on contact	Some adhesion on contact
	Release volume	0.0544 μL	0.0942 μL
	Release duration	0.4 seconds	1 minute
	Minute volume of susceptible subjects	11.8 L/min	7.5 L/min
	Heat output of subjects	70W/subject	15W/subject in 96% of cases, 55W/subject otherwise
	Index subject wearing a surgical mask	Off	Off in 73% of cases
Results	Exposure (% of release), Average	0.05% for 77% flow rate, 0.05% overall	0.01%
	Exposure (% of release), Maximum	0.24% for 77% flow rate, 0.30% overall	0.22%
	Coefficient of variance, Maximum	45%	15%
	Coefficient of variance, Average	5.4%	9.2%

Limitations

Cases studied in the present work were intended to be representative of the typical cabin environment. However, the effects of most of the factors that are expected to affect material transport have not been studied, either here or elsewhere. The following uncharacterized effects are expected:

- The cabin configuration affects the airflow pattern, which varies somewhat throughout the cabin. The cabin configuration includes selections made by the airline operator, such as the seating arrangement for First and Business class and the class divider, galley separators, and lavatory locations. It also includes temporary modifications made by the passengers, such as the use and position of Personal Air Outlets, the position of tray tables and stow bins, the reclined or upright seat positions, the presence of under-seat luggage, and the level of passenger loading. In addition, seat geometry and pitch may affect the particle content in the breathing zones of susceptible subjects.

- The on-ground cabin environment defined by the operator and the airport, including temperature and humidity, is expected to affect particle dynamics and may affect the airflow pattern. During boarding and deplaning, the aircraft engines must be turned off, and the APU may be required to be turned off by airport regulations, such that the operator is responsible for providing air conditioning via ground-based sources. When no efficient ground-based conditioning is available, temperature and humidity may deviate significantly from the values studied. (However, recirculated air continues to be provided at the 55% level included in this study.)

- Further, during boarding and deplaning, the entry door is open and the passengers and flight crew move around the cabin, which significantly alters the airflow pattern. Subject movements also occur during meal service and to use the lavatories. In addition to airflow, subject movements change the spatial relationships between index and susceptible subjects, as do variations in the subjects' seated postures.

- The use of masks and other face coverings capture a fraction of the expiratory material and redirect the flow of the remainder.

These factors combine to create infinite permutations. However, an exhaustive case exploration is not required to generalize the results of the current study. Data from the present model shows that some exposure onboard aircraft can occur, so vulnerable populations are advised to remain

vigilant; but, the level of exposure appears to be low under the most representative circumstances, consistent with both the experimental work by TRANSCOM/AMC [8], and the absence of confirmed transmissions due to air travel within the U.S. [1].

Methods

Particle Generation

The cough bioaerosol was modeled using the particle size distribution, particle count, and material volume obtained by Zayas *et al.* [9], which is consistent in shape with the dataset from Morawska *et al.* [10]. While a very wide range of distributions and concentrations exists in the current literature, the Zayas *et al.* dataset was selected because it was developed using a fast-acquisition and high-resolution laser diffraction system that enabled the team to identify very small particles at a high particle density. In contrast, many literature reports have a minimum bound of 0.37 μm which, based on the Zayas *et al.* dataset, would have the effect of undercounting 99.8% of particles and 27% of particle volume, even if the lower bound were due to simple truncation. However, the volumetric undercount due to less rigorous methodology is expected to be even higher, because particles that are counted in many studies evaporate before the count takes place.

Of the two distributions reported by Zayas *et al.*, the dataset without the outlier (superemitter) was used. Superemission was not considered in this study; however, due to the need for computational simplification described in the following section, the choice of a superemitter would not have affected results. Since the data were reported as particles per cm^3, values were multiplied by the instrument analysis volume of 7.85 cm^3. This brought the total particle count to approximately 106M for a reported material volume of 0.0544 μL. (In contrast, some current literature reports include particle counts in the tens of thousands). No correction was made to account for the distance from the mouth of the subject to the instrument sensor, which was 17 cm. The resulting particle size distribution is shown in Supplementary Fig. S7.

Cough flow dynamics were modeled using the methodology of Gupta *et al.* [11]. The arbitrarily selected inputs of cough peak flow rate of 3.67 L/s, cough expired volume of 0.7 L, and peak velocity time of 76.2 ms were used to generate the cough profile, which was truncated at 0.4 seconds (or 10% of the cough peak flow rate) and is shown in Supplementary Fig. S8. A mouth opening area of 4 cm^2 was used, and a single cough angle of 27.5° was used as average of the 95% confidence interval values provided by Gupta *et al.*

Particle Dynamics

Computational Fluid Dynamics modeling was conducted using Ansys Fluent 19.2 software. Thermal boundary conditions, listed in Supplementary Table S2, were selected to maintain the cabin temperature at the passenger-preferred 75°F while maintaining the airflow rates of interest. Composition of the continuous phase (the mixture of air and water vapor) was solved using the Eulerian scheme, which accounted for interactions between expiratory particles and the surrounding medium, including heat transfer and evaporation. In this scheme, expiratory particles were modeled as water with a volatile fraction of 90%. However, their vapor pressure was adjusted by a factor of 0.28 to account for the effect of pulmonary surfactants [12]. Using this approach, particles evaporated gradually over about 1 second until reaching 10% of their initial size.

Steady-state solutions over 13.3M polyhedral mesh cells were used as the initial conditions for the subsequent transient simulations. A time step of 0.05 seconds was used after the initial impulsive event which was calculated using shorter time steps. Transport equations in the continuous phase were solved using the realizable k-ε turbulence model with enhanced wall treatment. Transport equations of expiratory particles were solved using the Lagrangian discrete phase model. To reduce computational complexity, the volume of each cough was scaled down by a factor of 157 from a total of 106M particles to 676,208, and was scaled back at the end of the simulations for post-processing. Particles were tracked in parcels, or statistical representations of individual droplets, of an average of 19.57 particles each, for an average of 34,555 parcels per simulation. On contact with surfaces, particles were deposited with complete efficiency to account for the effect of pulmonary surfactants [13].

Particle Inhalation

Particles were assumed to have evaporated to their nonvolatile fractions by the time they reached the nearby breathing zones. This is a conservative assumption: if inaccurate, reported values would overestimate actual exposures. As the first post-processing step, the nonvolatile volume of particles in each breathing zone was determined by taking the total mass of particles and converting it to volume using the density of water.

For each passenger, the inhalation portion of a sinusoidal tidal breathing curve was calculated as follows:

$$V_{tidal,i}(t) = \begin{cases} A\ \sin(B(t+C)), 0 < B(t+C) < \pi \\ 0, \pi \leq B(t+C) \leq 2\pi \end{cases} \quad (1)$$

Using equations provided by Gupta *et al.* [14], A was taken as 0.616 L/s and B as 2.23 s^{-1}, assuming an average U.S. male with a weight of 89.7 kg and height of 1.75 m [15]. This was a conservative choice, since the minute volume for an average U.S. male is about 25% higher than that for an average U.S. female. The phase shift C was varied for each passenger to obtain the maximum nonvolatile volume inhaled. An example inhalation curve is shown in Supplementary Fig. S9.

The well-mixed model was applied to each breathing zone as a simplifying assumption that is not expected to bias results. The nonvolatile volume of particles in the breathing zone at a given time, $V_{bz,p}(t)$, was divided by the total 22.7 L volume of the breathing zone, $V_{bz,tot}$, to get the nonvolatile particle fraction in the breathing zone, multiplied by the time-dependent tidal inhalation volume $V_{tidal,i}(t)$, and then integrated over the time of the simulation t_s as follows:

$$V_{p,i} = \int_0^{t_s} V_{tidal,i}(t) \frac{V_{bz,p}(t)}{V_{bz,tot}} \, dt \qquad (2)$$

Results of example calculations are shown in Supplementary Fig. S9.

Data analysis and plotting were performed in Excel 2013, MATLAB R2019b, and JMP14.

Data Availability

All inputs and outputs reported in this paper are provided either in the main text or as Supplementary Information, which includes both graphical representations and Excel files of tabular data. Researchers are encouraged to contact the corresponding author for clarifications, advice on data utilization, and collaborations.

References

1. Duncan, I. Nearly 11,000 people have been exposed to the coronavirus on flights, the CDC says. *The Washington Post* https:\\www.washingtonpost.com/local/trafficandcommuting/nearly-11000-people-have-been-exposed-to-the-coronavirus-on-flights-the-cdc-says/2020/09/19/d609adbc-ed27-11ea-99a1-71343d03bc29_story.html (2020).

2. Center for Disease Control and Prevention (CDC), COVID-19, Symptoms of coronavirus. *CDC* https://www.cdc.gov/coronavirus/2019-ncov/symptoms-testing/symptoms.html (2020).

3. Tritton, D. J. The Coandă Effect in *Physical Fluid Dynamics*, 284-286 (Springer Netherlands, 1977).

4. Lindsley, W. G. *et al.* Measurements of airborne influenza virus in aerosol particles from human coughs. *PLOS ONE* **5**, e15100; 10.1371/journal.pone.0015100 (2010).

5. Milton, D. K., Fabian, M. P., Cowling, B. J., Grantham, M. L., McDevitt, J. J. Influenza virus aerosols in human exhaled breath: particle size, culturability, and effect of surgical masks. *PLOS Pathog*. **9**, e1003205; 10.1371/journal.ppat.1003205 (2013).

6. Leung, N. H. L., *et al.* Respiratory virus shedding in exhaled breath and efficacy of face masks. *Nat. Med.* **26**, 676-680 (2020).

7. Tellier, R. Review of aerosol transmission of influenza A virus. *Emerg. Infect. Dis.* **12**, 1657-1662 (2006).

8. Silcott, D. *et al.* TRANSCOM/AMC commercial aircraft cabin aerosol dispersion tests. *TRANSCOM* https://www.ustranscom.mil/cmd/docs/TRANSCOM%20Report%20Final.pdf (2020).

9. Zayas, G. *et al.* Cough aerosol in healthy participants: fundamental knowledge to optimize droplet-spread infectious respiratory disease management. *BMC Pulm. Med.* **12,** 11; 10.1186/1471-2466-12-11 (2012).

10. Morawska, L., *et al.* Size distribution and sites of origin of droplets expelled from the human respiratory tract during expiratory activities. *J. Aerosol Sci.* **40**, 256-269 (2009).

11. Gupta, J. K., Lin, C.-H., Chen, Q. Flow dynamics and characterization of a cough. *Indoor Air* **19**, 517–525 (2009).

12. Vejerano, E. P., Marr, L. C. Physico-chemical characteristics of evaporating respiratory fluid droplets. *J. R. Soc. Interface* **15**, 20170939; 10.1098/rsif.2017.0939 (2018)

13. Olson, N. A., Skogerboe, K. J., Synovec, R. E. Hydrophobic interaction chromatography coupled with dynamic surface tension detection for the determination of surface active species in protein formulations. *J. Chromatogr. A* **806**, 239-250 (1998).

14. Gupta, J. K. Respiratory exhalation/inhalation models and prediction of airborne infection risk in an aircraft cabin. *Purdue e-Pubs* https://docs.lib.purdue.edu/dissertations/AAI3449758/ (2010).

15. CDC, National Center for Health Statistics, Body Measurements, *CDC* https://www.cdc.gov/nchs/fastats/body-measurements.htm (2020).

Acknowledgements

The authors thank Chao-Hsin Lin, Matthew J. Schwab, and Robert J. Atmur for many productive discussions on the Environmental Control System, CFD modeling, and the content of this paper. The authors thank the High Performance Computing staff at Boeing who prioritized access to computing resources for this activity and provided around-the-clock server support. The authors acknowledge Ansys for providing licenses for their Fluent software to support Confident Travel Initiative studies at Boeing.

Author Contributions

ACD, ADC, TW, SPJ, LLW, and NAO designed the experiments and set the methodologies.

TW, ADC, ACD and NAO provided parameterization prior to TW and ADC performing computational fluid dynamics calculations.

ACD, ADC, TW, and NAO performed data analysis and validated the data content.

ACD, ADC, TW, and NAO wrote sections of the original draft and edited the document.

ACD, MZ, and NAO curated the data.

MZ wrote and edited the original draft and all subsequent versions of the paper.

ADC and JJC provided resources including access to off-the-shelf software, software licenses, configuration parameters, labor, and computational resources.

JJC provided supervision, administration, and acquisition of funding.

NAO as corresponding author ensured that original data upon which the submission is based is preserved and retrievable for reanalysis, approved data presentation as representative of the original data, and has foreseen and minimized obstacles to the sharing of data described in the work.

Competing Interests

All authors are employees of The Boeing Company and have no other competing interests. Funding and other resources for this work were provided by The Boeing Company. In-kind contribution was provided by Ansys through supply of licenses for Fluent software.

Figure Legends

Fig. 1. Airflow design in narrow-body aircraft. (a) Airflow delivery features in the 737 Boeing Sky Interior cabin used in simulations. (b) Idealized airflow pattern in the passenger cabin.

Fig. 2. Velocity vectors of initial conditions at 100% flow rate with the highest velocities shown in red and the lowest ones in blue. Time offset and initial condition index as follows: (a) 0 s, Initial Condition 1, (b) 90 s, Initial Condition 2, (c) 120 s, Initial Condition 3.

Fig. 3. Decay of expiratory particles over time after initial release. (a) Airflow at 100% with different index seats and initial conditions. (b) Airflow at 55-100% with index subject in aisle seat 3D.

Fig. 4. Mass of expiratory material released by index passenger in middle seat 3E and present in the breathing zones of susceptible subjects in nearby seats over time after initial release.

Fig. 5. Seat chart for the 5-row section used in the model, highlighting seats occupied by the index subject in different simulations.

Fig. 6. Mass of expiratory material inhaled by susceptible subjects in different seats for different airflow conditions (a-c) and different index passenger seat positions at 100% airflow (a, d-e). Error bars in (a) represent the range over three different initial conditions.